RSC Advances

PAPER

View Article Online
View Journal | View Issue

Cite this: *RSC Adv.*, 2025, **15**, 13951

Research on electrochemical chiral sensors constructed based on the intrinsic chiral characteristics of AuNPs†

Yuping Zhu, *[a] Yong Yan,[b] Ruo Yuan [c] and Haijiao Xie[d]

Nanogold particles inherently possess chiral characteristics. As chiral selectors, they can recognize amino acid enantiomers. *Ab initio* molecular dynamics (AIMD) simulations were employed to explore the interaction mechanism between gold nanoparticles and D/L-phenylalanine. Additionally, the binding energies of gold nanoparticles with D-phenylalanine and L-phenylalanine were calculated respectively. On the basis of the calculation results, gold nanoparticles were combined with graphene oxide/thionine to form a nanocomposite, which was used to modify the surface of a gold electrode for the recognition of D/L-phenylalanine. Scanning Electron Microscopy (SEM), ultraviolet-visible spectroscopy (UV-vis), and circular dichroism (CD) were utilized to characterize and analyze graphene oxide, thionine, gold nanoparticles, and the graphene oxide/thionine/gold nanoparticle composite material. Electrochemical cyclic voltammetry was used in the construction process and performance characterization of this chiral sensor. Under the same experimental conditions, the electrode modified with the graphene oxide/thionine/gold nanoparticle composite exhibits different current response signals for D/L-phenylalanine. The current response of the binding reaction between nano-gold and D-phenylalanine is stronger than that of L-phenylalanine. The experimental results are consistent with the simulation calculation results. This electrochemical chiral recognition method provides a new strategy for the recognition of chiral enantiomers.

Received 23rd February 2025
Accepted 22nd April 2025

DOI: 10.1039/d5ra01303h

rsc.li/rsc-advances

Introduction

The recognition of enantiomers is of great significance in chemical and biological research. In the past few decades, numerous strategies have emerged, ranging from instrumental methods to material sources, providing a wealth of analytical methods for the recognition of chiral enantiomers.[1–10] These methods include chromatography,[11] mass spectrometry,[12] colorimetry,[13] spectroscopy,[14] extraction,[15] capillary electrophoresis,[16] and nuclear magnetic resonance,[17] among others. Electrochemical chiral recognition is based on the detection of changes in current or potential caused by the interaction at the sensor/chiral molecule interface.[18] Compared with other methods, electrochemical methods have attracted much attention due to their high sensitivity, simple operation, rapid detection, and low cost.[8–10] The key to constructing an electrochemical chiral sensor lies in creating a chiral surface with enantiomer recognition sites on the electrode, which can generate different electrochemical responses to the two enantiomers.

Phenylalanine (Phe) has two enantiomers, D-Phe and L-Phe (Scheme 1). D-Phe can enhance the body's immune function and has excellent analgesic effects. It is commonly used in the production of medications such as buphenine and nalgeina.[19] L-Phe is one of the eight essential amino acids that cannot be synthesized in human and animal bodies. It is also an important component of aspartame, a new high-sweetness and low-

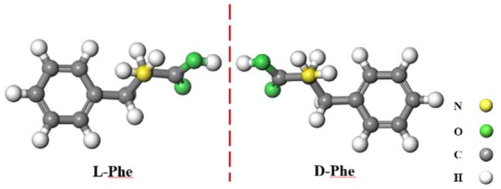

Scheme 1 Structure of D/L-Phe.

[a]*College of Chemistry and Chemical Engineering, Neijiang Normal University, Neijiang, 641100, P. R. China*
[b]*School of Chemistry and Chemical Engineering, Guangxi University, Nanning 530005, P.R. China*
[c]*Key Laboratory of Luminescence Analysis and Molecular Sensing (Southwest University), Ministry of Education, College of Chemistry and Chemical Engineering, Southwest University, Chongqing 400715, P. R. China. E-mail: yuanruo@swu.edu.cn; Fax: +86-23-68253172; Tel: +86-23-68252277*
[d]*Hangzhou Yanqu Information Technology Co., Ltd Y2, 2nd Floor, Buiding 2, Xixi Legu Creative Pioneering Park, No. 712 Wen'er West Road, Xihu District, Hangzhou City, Zhejiang Province, 310003, P. R. China*

† Electronic supplementary information (ESI) available. See DOI: https://doi.org/10.1039/d5ra01303h

calorie sweetener.[20–22] Therefore, the detection of phenylalanine enantiomers carries significant importance.

Metal complexes, as a typical class of chiral selectors, are commonly used for the chiral recognition of phenylalanine tryptophan, and amino acid derivatives. In this experiment, we utilized the inherent chiral characteristics of AuNPs to recognize Phe, eliminating the need for metal complexes as chiral selectors and bypassing the ligand exchange process between enantiomers and chiral selector complexes. The interaction modes and binding strengths between AuNPs and D/L-Phe were simulated and calculated using the VASP (Vienna *Ab initio* Simulation Package) software to investigate the primary mechanisms underlying the chiral recognition of D/L-Phe by AuPNs.

GO is a new type of carbon material with excellent properties such as high electrical conductivity, thermal conductivity, stability, large specific surface area, and good biocompatibility.[23,24] GO is rich in oxygen-containing functional groups such as hydroxyl, carboxyl and epoxy groups.[25–28] These functional groups not only provide an effective sensing platform for electrochemical sensors, but also amplify the electrical signal to improve the detection sensitivity of the sensor.[29] Thi is a redox dye composed of two aromatic rings, one heterocycle, and two amino groups. Both GO and Thi contain conjugated π-electron systems, GO exhibits a synergistic effect of π–π stacking and non covalent charge transfer effect.[30,31] Thi is embedded on the surface of GO through π–π conjugation (analogous to hydrogen bonding). Since GO carries a negative charge, the positively charged Thi can easily intercalate into the interlayer spaces *via* electrostatic adsorption, thereby expanding the interlayer distance. This expansion creates favorable conditions for the loading of AuNPs.[32–46] This noat only improves the dispersibility of GO but also enables effective immobilization of Thi. The amino groups of Thi combine with the gold atoms of AuNPs to form Au–N bonds, preparing the GO/Thi/AuNPs composite material (Scheme 2). This composite is modified on the electrode surface to recognize D/L-Phe. Based on the above rationale, an electrochemical chiral sensor was designed with AuNPs as the chiral selector and GO and Thi as the electrode immobilization materials.

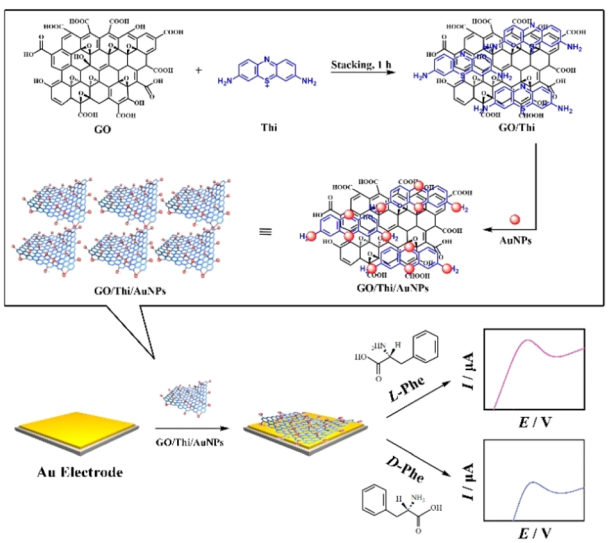

Scheme 2 Schematic illustration of preparation process of the immunosensor.

Results and discussion

DFT calculations on the recognition of phenylalanine by AuNPs

AuNPs are frequently used for chiral recognition. Typically, chiral selection reagents are coated on the surface of AuNPs to confer chirality to the nanoparticles.[37] Ref. 38 reports, chiral character of AuNPs, there were few reports on the specific mechanism and deep – seated reasons for the self – recognition of amino acids by nanogolds. In this study, the Vienna *Ab initio* Simulation Package (VASP) software[39–42] was used to simulate and calculate the interaction mode and intensity between AuNPs and D/L-phenylalanine, and to explore the main reasons for the recognition of D/L-phenylalanine by AuNPs. The configuration optimization of the gold nanoparticle (AuNPs) surface was performed first. The Au-111 facet of AuNPs (shown in Fig. S1†) was selected for binding energy calculations. The optimized D/L-Phe monomers were respectively combined with the Au-111 of AuNPs. The two optimized binding configurations under the same calculation level are shown in Fig. 1. When D-Phe binds to AuNPs, the benzene ring structure of D-Phe adopts a "parallel" orientation. That is, the six carbon atoms of the benzene ring are almost at the same distance from the AuNPs, as shown on the Fig. 1 (left). When L-Phe binds to AuNPs, the benzene ring structure of L-Phe adopts an "upright" orientation. That is, the six carbon atoms of the benzene ring are significantly different in distance from the AuNPs, as shown on the Fig. 1 (right).

The specific calculation methods in the VASP software are provided in the ESI.† For the adsorption reaction of molecules, the energy is calculated through the following equations:

$$E_{ad} = E_{sur+adsorbate} - E_{sur} - E_{adsorbate}$$

where $E_{sur+adsorbate}$ is the total energy of adsorption model, E_{sur} is the total energy of surface and $E_{adsorbate}$ is the total energy of adsorbate. The calculation results show that the adsorption energy of AuNPs-111 for D-phe is −1.49 eV, the adsorption energy of AuNPs-111 for D-phe is −1.16 eV. The more negative

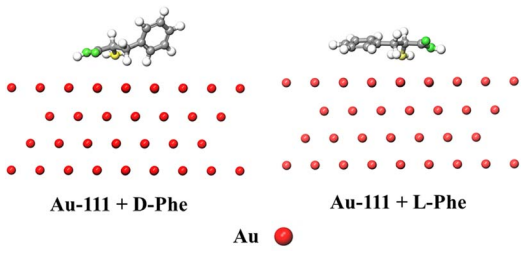

Fig. 1 The interaction modes between Au-111 of AuNPs and D/L-phenylalanine.

the adsorption energy, the easier it is to adsorb, therefore, the ability of AuNPs to adsorb D-Phe is stronger than L-Phe.

Morphologies of the GO and GO/Thi nanocomposites

The surface morphologies of GO and GO/Thi nanocomposites were investigated using SEM as shown in Fig. 2. The SEM image in Fig. 1 (left) showed that graphene oxide exhibits a twisted sheet structure of single-layer or few-layer, with wrinkled edges. This indicates that a large number of oxygen-containing functional groups formed on the surface and edges of graphene oxide sheets during the oxidation process, which to some extent destroys the original π-conjugated structure of graphene and causes lattice defects on the surface. The formation of these wrinkles and bends is conducive to the stability of the two-dimensional structure of GO. After thionine modification, it can be seen from Fig. 1 (right) that the GO/Thi composite still shows wrinkles, with a large-area gauze-like organizational structure. The edge parts of the material are wrinkled, and the boundary presents an irregular lamellar structure. This is because Thi is positively charged, and the electrostatic repulsion between the functionalized GO sheets can overcome the van der Waals forces and prevent their agglomeration, confirming that the GO/Thi nanocomposites are not flat and compact structures. Fig. 1 shows the cross-sectional SEM image of the GO/Thi/AuNPs composites film. The image reveals that the composite film exhibits good thickness uniformity, though slight variations exist due to the fluidity of the composite solution during film formation. The average thickness of the film is approximately 30 μm.

UV-visible spectra of various materials

The UV-vis absorption spectra (Fig. 3A, curves a–d) confirmed the successful synthesis of AuNPs with sizes of 4 nm, 10 nm, 16 nm, and 30 nm. As shown in Fig. 3A, the localized surface plasmon resonance absorption peak of AuNPs appeared around 520 nm.[43,44] 4 nm AuNPs showed a relatively weak localized surface plasmon resonance (LSPR) peak at 515–520 nm, and the sample appeared golden-yellow. Both 10 nm and 16 nm AuNPs exhibited a strong LSPR peak at 520 nm, with the samples displaying a wine-red color. For 30 nm AuNPs, the LSPR peak underwent a blue shift, and the sample turned light purple. According to Mie theory,[45] as the diameter of AuNPs increases, the UV-vis absorption peak of gold colloids broadens and red-shifts (moves toward longer wavelengths).

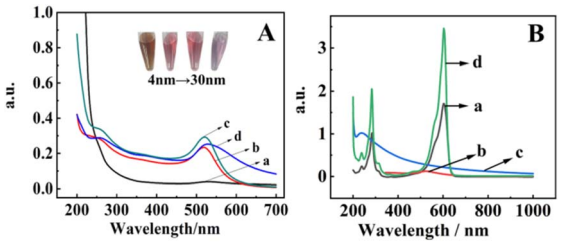

Fig. 3 (A) UV-vis absorption spectra of a nanoparticles with four different particle sizes. (B) UV-vis spectra of Thi, AuNPs, graphene oxide, and GO/Thi/AuNPs composites.

Fig. 3B presents the UV-vis spectra of Thi, 16 nm AuNPs, graphene oxide, and GO/Thi/AuNPs composites. The optical absorption shown in the UV-vis spectrum (Fig. 3B, curve a) revealed that the λ_{max} of Thi were 284 and 603 nm, the λ_{max} of AuNPs were 523 nm (Fig. 3B, curve b), the λ_{max} of GO were 239 nm (Fig. 3B, curve c). The results are basically consistent with the reported data. There were basically the same λ (238 nm, 283 nm and 603 nm, curve 2d) of GO/Thi/AuNPs compared to that of Thi and GO respectively. The λ (563 nm) of GO/Thi/AuNPs had a blue shift compared to that of AuNPs respectively, which could be ascribed to the π–π conjugation effect between GO and AuNPs.This indicates that the complex has been successfully prepared.

Chiral characterization of materials

Circular dichroism (CD) spectroscopy is an optical rotation spectroscopy used to determine the configuration and conformation of asymmetric molecules. In this experiment, CD spectra were measured for AuNPs (with particle sizes of 4 nm, 10 nm, 16 nm and 30 nm) and L/D-Phe. The CD spectra of AuNPs all exhibited negative signals to varying degrees. The CD spectrum of D-Phe showed a negative signal, while that of L-Phe displayed a positive signal. Fig. 4A shows the CD spectrum of 16 nm AuNPs. Fig. 4B presents the CD spectra of D-Phe and L-Phe. After adding D-Phe or L-Phe separately to AuNPs solutions of different sizes, the mixtures were allowed to react completely, followed by centrifugation. The supernatant was discarded, and the precipitate was redispersed in deionized water to the original volume for CD spectral measurement. The results indicate that D-Phe interacted with AuNPs of different sizes, producing negative chiral signals. L-Phe showed much weaker interaction with AuNPs, exhibiting almost no chiral signal compared to D-

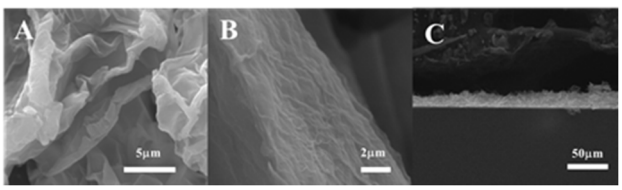

Fig. 2 SEM images of (A) GO at low magnification of 5 μm, (B) GO/thionine nanocomposites at low magnification of 2 μm, and (C) film thickness of the GO/thionine/AuNPs at low magnification (50 μm).

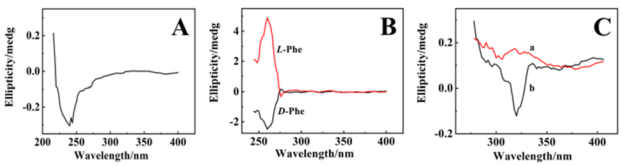

Fig. 4 (A) CD spectrum of 16 nm AuNPs, (B) CD spectrum of D/L-Phe, (C) CD spectra of the precipitates after reaction of AuNPs with either D-Phe or L-Phe, followed by centrifugation and supernatant removal, (a) L-Phe + GO/Thi/AuNPs, (b) D-Phe + GO/Thi/AuNPs.

Phe (Fig. 4C). It is speculated that this phenomenon occurs because A and D-P share the same optical rotation direction. In chiral recognition, homotypic interactions proceed faster, while heterotypic interactions are slower.[46] These results are consistent with first-principles DFT calculations.

Electrochemical characterizations of the modified electrode

To illustrate the electrochemical signal intensity of the composite material and its binding degree with L/D phenylalanine, cyclic voltammetry was used to characterize the electrode modification process, the results were shown in Fig. 5. Curve 5a was the cyclic voltammetry curve of the bare gold electrode, there were no redox peaks in the test bottom solution, which was because there were no electroactive substances on the electrode surface or in the test bottom solution. Curve 5b was the cyclic voltammetry curve of the gold electrode modified with GO/Thi/AuNPs in the test bottom solution. At this time, a pair of quasi-reversible redox peaks appear. It was because thionine in the composite material was an excellent electron mediator that can accelerate electron transfer. Two gold electrodes simultaneously modified with the GO/Thi/AuNPs composite were immersed in 10.0 mL of 5 mmol per L L-Phe and D-Phe solutions respectively for 15 minutes,the test results were shown in curve 5c and d, compared with the cyclic voltammetry curve of the modified electrode, the shapes of curves 5c and d remain symmetric, and the positions of the redox peaks are only slightly shifted. The redox values of curves 5c and d were both lower than those of the CV curve of the electrode modified with the composite material, indicating that the modified electrode has a certain degree of binding with D/L-Phe. Notely, the redox peak current value of the CV curve 5d after the binding of the modified electrode with D-Phe decreases more significantly than L-Phe (curve 5c), indicating that the chiral selector, gold nanoparticles, has a stronger binding ability for D-Phe.

Comparison of electrochemical properties of electrodes modified with graphene oxide/thionine/gold nanoparticle composites

In order to compare the electrochemical signals of the composite materials without graphene oxide, the cyclic voltammetry curve of Thi/AuNPs/Au was tested, as shown in Fig. 6. Curve 6a was the CV curve of the gold electrode modified with

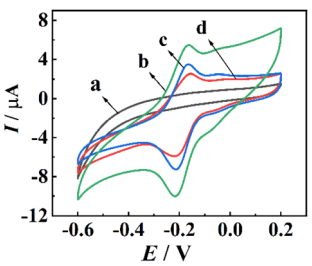

Fig. 5 Cyclic voltammogram of the electrode during the modification process, (a) bare gold electrode, (b) (GO/thionine/AuNPs)/Au. (c) L-Phe/(GO/thionine/AuNPs)/Au. (d) D-Phe/(GO/thionine/AuNPs)/Au.

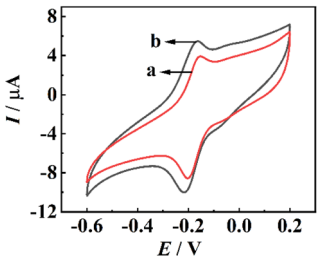

Fig. 6 CV of gold electrodes modified with different modifying materials. (a) Thi/AuNPs/Au, (b) (GO/Thi/AuNPs)/Au.

Thi/AuNPs/Au. The current value of redox peak was lower than curve 6b of the gold electrode modified with GO/Thi/AuNPs. This indicates that the presence of graphene oxide increases the loading amount of thionine and gold nanoparticles on the electrode. While enhancing electron transfer, more chiral selectors were also fixed per unit area.

On the other hand, galvanostatic charge–discharge (GCD) measurements were utilized to gain a detailed understanding of the voltammetric behaviours of the GO/thionine/AuNPs hybrids modified electrode with D-Phe. Its electrochemical curves at different scan rates (50, 80, 100, 150, 200, 300, and 400 mV s^{-1}) in the range of −0.6–0.2 V were obtained as shown in Fig. 7(A). The electrochemical reversibility of the aforesaid electrode remained with increasing scan rates, but the redox peak positions were just shifted slightly and the redox peak current values changed dramatically. Specially, the linear relationships between the oxidation/reduction peak current values and the scan rates were found Fig. 7(B), respectively. Linear relationship for the oxidation peak was measured as $I_a = 0.04221\nu + 1.49712$. Linear relationship for the reduction peak was measured as $I_b = -0.06371\nu - 4.63391$. These results suggested that the GO/thionine/AuNPs hybrids modified electrode could be used for quantitative detection of D-Phe.

The influence of AuNPs size on hand recognition performance

To investigate the effect of particle size AuNPs on the chiral recognition performance of D/L-Phe, four different sizes of AuNPs (4 nm, 10 nm, 16 nm, and 30 nm) were prepared and

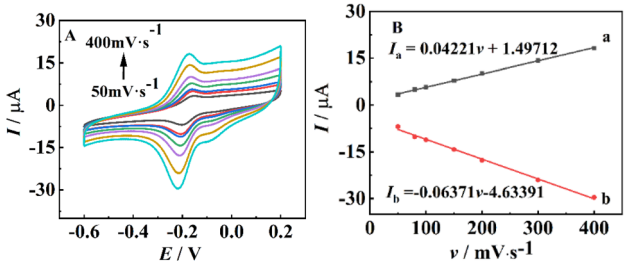

Fig. 7 Cyclic voltammograms obtained from the GO/thionine/AuNPs hybrids modified electrode with L-Phe at different scan rates in a a testing base solution containing 0.1 mol per L NaAc-HAc (A). Linear relationship between the oxidation (a)/reduction (b) peak current values and the scan rates (B).

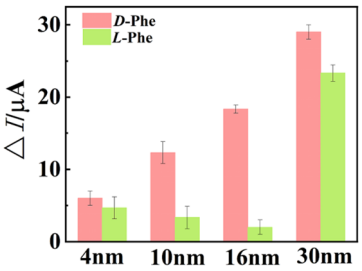

Fig. 8 The chiral recognition of D/L-Phe by AuNPs with different particle sizes.

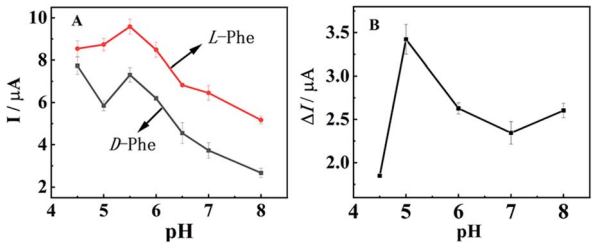

Fig. 9 Effect of pH on D/L-Phe recognition (A). Dependence of ΔI on pH (B).

modified on electrodes for the recognition of D/L-Phe. The recognition performance was characterized by CV, where the difference in peak current before and after recognition ΔI ($\Delta I = I_{\text{AuNPs+D/L-Phe}} - I_{\text{AuNPs}}$) was measured. A larger ΔI value indicates stronger adsorption of D/L-Phe by AuNPs and more significant interaction. The experimental results are shown in the Fig. 8. Fig. 8, shows that for all four particle sizes of AuNPs, the interaction with D-Phe is stronger than with L-Phe. Among them, the 16 nm AuNPs exhibits the largest ΔI difference between its interactions with D-Phe or L-Phe, indicating the best chiral recognition performance. This is primarily because the synthesis of AuNPs is influenced by multiple factors, leading to diverse arrangements of metal atoms. Consequently, the chiral properties of AuNPs vary with particle size.

The effect of the pH of the test solution on the modified electrodes

The pH of the solution plays an important role in enantiospecificity of D/L-Phe enantiomers. Two modified electrodes were reacted with 5 mmol per L D/L-Phe solutions for 15 minutes in sequence, their response current values were then measured in different pH (3.5, 4.0, 4.5, 5.0, 5.5, 6.0, 6.5, 7.0, 8.0, 8.5) electrolytes (Fig. 9A). It can be seen that the maximum difference of peak current between two enantiomers appeared at pH 5.0 (Fig. 6B). So pH 5.0 was selected for the experiment.

The effect of electrode incubation time

The two modified electrodes were respectively placed in D-Phe and L-Phe solutions and reacted for 5 min, 10 min, 15 min, 20 min, 25 min, 30 min, 35 min, 40 min, 45 min, 50 min, 55 min, 60 min, and 65 min. The oxidation and reduction peak current responses of D-Phe and L-Phe increased with increasing reaction time (Fig. 10A). It can be seen that the maximum difference of peak current between two enantiomers occurred at a reaction time of 45 min (Fig. 10B). Therefore, a reaction time of 45 min was chosen for the experiment.

Electrochemical response performance of the chiral sensor

Quantitative detection of phenylalanine enantiomers by modified electrodes under optimized experimental conditions.

As shown in Fig. 11A, the difference in oxidation peak current was linearly related to the D/L-Phe concentration within 2 to 8 mmol L^{-1}, while the regression equation were as follows respectively: $\Delta I = 3.72225c - 1.87039$ and $\Delta I = 1.63861c - 0.27075$.

As can be seen from the Fig. 11A, there were obvious differences in the current changes caused by L-Phe and D-Phe. ΔI_L is always greater than ΔI_D, further indicating that the GO/Thi/AuNPs modified surface was more likely to adsorb L-Phe. Fig. 11B and C illustrates that with increasing concentration of D/L-Phe from 2 to 8 mmol L^{-1}, the current signals were gradually enhanced.

Applications of chiral sensors

To demonstrate the application value of the constructed electrochemical chiral sensor, the modified electrode was used to detect a series of solutions in which L- and D-phenylalanine were mixed in different percentages. Fig. 12 shows the differences in the relative peak currents after the reaction of (GO/Thi/AuNPs)/Au with mixed solutions of L-and D-phenylalanine in different ratios. The change in peak current gradually increases with the increase in the proportion of L-phenylalanine. The ratio of enantiomers in the mixed solution of L-phenylalanine and D-phenylalanine can be detected through a standard curve with good linearity.

Chiral sensor recognition of other amino acid enantiomers

To investigate the recognition capability of this chiral sensor for other amino acid enantiomers, four amino acids were selected, including phenylalanine, tryptophan, cysteine, and serine. The recognition performance was characterized by cyclic voltammetry (CV), measuring the peak current difference ΔI ($\Delta I = I_{(\text{GO/Thi/AuNPs+D/L-Phe})} - I_{(\text{GO/Thi/AuNPs})}$), a larger ΔI indicates stronger adsorption of the amino acid by the composite, more significant

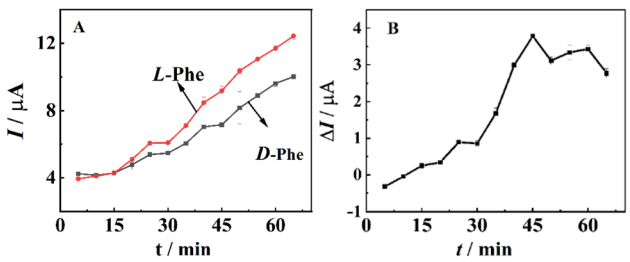

Fig. 10 The relationship of reaction time between modified electrode and D/L-Phe (A). Dependence of ΔI on incubation time (B).

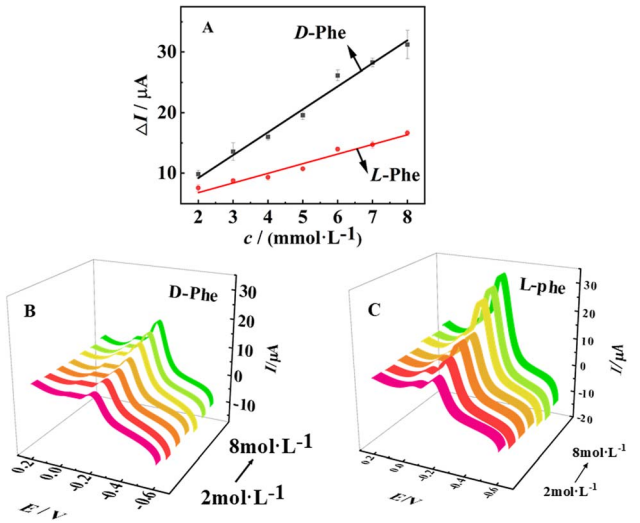

Fig. 11 Relationship diagram between peak current difference and D/L-Phe concentration (A). CV intensity of the biosensor in gradually enhanced D-Phe (B) and L-Phe (C) concentration (2 to 8 mmol L^{-1}).

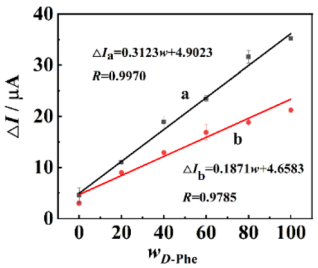

Fig. 12 Current changes in the reaction of (GO/Thi/AuNPs)/Au with a series of solutions in which D- and L-Phe are mixed in different ratios. The concentrations of Phe were: (a) 8 mmol L^{-1} and (b) 2 mmol L^{-1}.

interaction, and better enantiomeric discrimination (the greater the ΔI difference between the two enantiomers, the better the recognition performance). As shown in Fig. 13, the experimental results indicate that phenylalanine exhibits the better recognition performance, while tryptophan also shows a certain degree of recognizability. It is hypothesized that both phenylalanine and tryptophan are aromatic amino acids containing

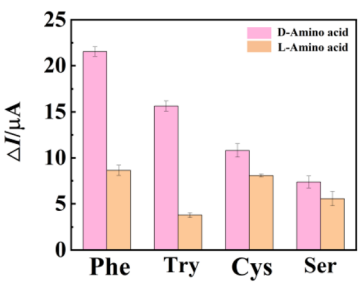

Fig. 13 Chiral sensor recognition of four amino acids.

benzene rings, enabling them to bind more tightly with the GO/Thi/AuNPs composites.

Experimental

Reagents and materials

Graphite power (G, 8000 mesh) was purchased from Nano Technology Ltd (Nanjing, China). $HAuCl_4$ was purchased from Sigma-Aldrich (China). D/L-phenylalanine, potassium persulfate, sodium acetate, anhydrous acetic acid, phosphorus pentoxide, concentrated sulfuric acid (H_2SO_4, 98%), sodium nitrate, potassium permanganate, hydrochloric acid, and hydrogen peroxide were purchased from Chemical Reagents Co., Ltd in China. All chemicals and solvents used were of analytical grade. Deionized (DI) water from a Milli-Q-MilliRho purification system (resistivity 18 M Ω cm) was used for the preparation of all solutions.

Apparatus

All electrochemical experiments were conducted with an electrochemical workstation (CHI660E), and utilized saturated calomel electrode (SCE) and platinum plate as a reference electrode and a counter electrode, respectively, in a three-electrode system. Cyclic voltammetry and amperometric experiments were performed with a three-electrode system using a bare or modified bare gold electrode (4.0 mm in diameter) as the working electrode, a platinum wire as auxiliary electrode, and a saturated calomel electrode (SCE) as reference electrode. All potentials were measured and reported *versus* the saturated Ag–AgCl electrode as reference electrode, the test solutions were 5 mL of PBS. The morphologies of the films were investigated with scanning electron microscopy (SEM, VEGA38BH Czech Republic). All experiments were carried out at room temperature.

Preparation of GO

GO was prepared by the oxidation of graphite powder according to Hummers' method.[47] Concentrated H_2SO_4 (30 mL) was added to a mixture of graphite powder (5 g) and $NaNO_3$ (2.5 g) in a three-necked flask, the mixture was stirred and cooled to 0 °C. Then, $KMnO_4$ (5 g) was added slowly in portions to keep the reaction temperature below 5 °C for 30 min. The mixture was heated to 40 °C for 10 h. Next, H_2O_2 (30% aqueous solution) was added to the mixture and stirred for 2 h until a brown-colored slurry was formed. Under ultrasonication, the GO suspension was washed by repeated filtration with 5% HCl aqueous solution and water until the pH of the solution became neutral. Finally, after vacuum drying, the GO nanosheets were obtained. The circular dichroism (CD) spectrometer was obtained from Applied Photophysics (Chirascan V100, UK).

Preparation of citrate-capped AuNPs

AuNPs were prepared according to previous reference by reducing $HAuCl_4 \cdot 4H_2O$ with citrate.[48] Briefly, 48 mL of water was mixed with 2 mL of 1% (w/w) $HAuCl_4$ solution to make the final concentration of $HAuCl_4 \cdot 4H_2O$ about 1 mM. Then, the

mixture was heated with stirring until it began to boil, and 1 mL (or 2 mL, 3 mL, 4 mL) of 5% trisodium citrate was added. Under continuous stirring and boiling, the mixture gradually changes to deep red, indicating the formation of AuNPs. Based on the absorbance value at position 524 on the UV-absorption spectrum and the molar extinction coefficient of AuNPs (2.7×10^8 M^{-1} cm^{-1}), the concentration of the synthesized AuNPs nanoparticles (with a diameter of 16 nm) was calculated to be 0.58 nM. After boiling for another 5 min, the solution was cooled to room temperature under vigorous stirring. The AuNPs were centrifuged by 12 000 rpm for 15 min, the precipitate was removed while the supernatant solution was collected for further use.

Preparation of GO/thionine nanocomposites

Ultrasonic agitation (for 1 h) was used to disperse the solid GO (5 mg) and thionine (5 mg) into DI water (5 mL). The mixture was stirred with a magnetic bar for 2 h. Then, the resulting suspension was centrifuged (3000 rpm, 5 min) to remove incompletely exfoliated GO and then centrifuged again (10 000 rpm, 15 min) to remove the dissociative thionine which undecorated on the GO sheets. The suspension of the GO/thionine nanocomposites was kept in a refrigerator at 4 °C for further use.

Preparation of GO/thionine/AuNPs hybrids

A composite of the GO/thionine nanocomposites and AuNPs (1 : 1/v/v) was vigorously stirred for 2 h. The GO/thionine/AuNPs hybrids were resuspended with DI water and kept in a refrigerator at 4 °C for further use.

Preparation of the modified electrodes

Initially, two gold electrodes (4.0 mm in diameter) were carefully polished on a microcloth pad using sequentially 0.3 μm and 1 μm alumina (Al_2O_3) slurries until a mirror-like shiny surface was obtained. Subsequently, the electrodes were ultrasonically cleaned with ultrapure water, absolute ethanol, and ultrapure water for 5 minutes each to remove alumina particles and other potential contaminants. The polished electrodes were then air-dried at room temperature.

After completing the polishing, cleaning, and drying procedures, 5 μL of the prepared GO/thionine/AuNPs nanocomposite suspension was drop-coated into the surfaces of the two treated electrodes and allowed to react at 25 °C for 4 hours. The prepared electrodes were stored in a refrigerator at 4 °C for subsequent use.

Conclusions

In this study, the VASP software was used to optimize the structures of AuNPs and D/L-Phe monomers, and the models of Au-111 of AuNPs binding to D/L-Phe were simulated. Specifically, when Au-111 of AuNPs binds to D-Phe, the benzene ring structure of D-Phe, adopts a "parallel" configuration; when Au-111 of AuNPs binds to L-Phe, the benzene ring structure of L-Phe adopts an "upright" configuration. Through calculations, it was found that the interaction mode between Au-111 of AuNPs and D/L-Phe is mainly of the adsorption type, and the adsorption intensity of AuNPs for D-Phe is greater than that for L-Phe. The different binding modes of Au-111 of AuNPs with D/L-Phe stem from the fact that AuNPs has a chiral nuclear center. On this basis,GO/Thi/AuNPs composites was prepared and used to modify a gold electrode, thereby constructing a novel current-based chiral sensor. Notably, the oxygen-containing functional groups on graphene oxide provide a large number of contact sites, enabling the electrode to adsorb more chiral selector nanogold particles per unit area and improving the detection sensitivity of the modified electrode. By modifying the redox probe Thi on the electrode surface, the step of adding electroactive substances to the test bottom solution was eliminated, simplifying the fabrication steps of the chiral sensor. Further validation through UV-absorption spectroscopy and circular dichroism spectra confirmed that AuNPs exhibits stronger interactions with D-Phe than with L-Phe, with GO/thionine/AuNPs composites solution containing nanoparticles of 16 nm in diameter showing more pronounced effects toward D-Phe. The experimental results were consistent with the simulation calculations. However, influenced by the size of AuNPs and the structural characteristics of amino acid enantiomers, this chiral sensor demonstrates superior detection performance for amino acids containing benzene ring structures. This strategy characterizes the electrode preparation and reaction process using cyclic voltammetry (CV), achieving the selective recognition of D/L-phenylalanine (D/L-Phe) enantiomers. Therefore, a novel electrochemical chiral enantiomer recognition method has been constructed. The experimental results are consistent with the simulation calculation results. This electrochemical chiral recognition method provides a new strategy for the recognition of chiral reagents.

Data availability

All data generated or analyzed during this study are included in this published article (and its ESI files†).

Author contributions

[Yuping Zhu]: investigation, data curation, funding acquisition, writing – original draft, writing – review and editing, validation; [Yong Yan]: data curation, writing – original draft, investigation; [Ruo Yuan]: formal analysis, methodology, resources; [Haijiao Xie]: software, methodology.

Conflicts of interest

There are no conflicts to declare.

Acknowledgements

We are grateful for the financial support from the Undergraduate Innovation Program in Neijiang Normal University (No. X2020059).

References

1 P. Lesot, C. Aroulanda, H. Zimmermann and Z. Luz, Enantiotopic discrimination in the NMR spectrum of prochiral solutes in chiral liquid crystals, *Chem. Soc. Rev.*, 2015, **44**, 2330–2375.
2 M. Weh, K. Shoyama and F. Würthner, Preferential molecular recognition of heterochiral guests within a cyclophane receptor, *Nat. Commun.*, 2023, **14**, 243.
3 Y. Zhu, X. Wu, S. Gu and L. Pu, Free amino acid recognition: A bisbinaphthyl-based fluorescent probe with high enantioselectivity, *J. Am. Chem. Soc.*, 2019, **141**, 175–181.
4 C. Han and H. Li, Chiral recognition of amino acids based on cyclodextrin-capped quantum dots, *Small*, 2008, **4**, 1344–1350.
5 P. Cai, D. Wu, X. Zhao and Y. Pan, Fluorescence recognition of chiral amino alcohols by using a novel ionic liquid sensor, *Analyst*, 2017, **142**, 2961–2966.
6 Z. A. D. l. Santos, S. MacAvaney, K. Russell and C. Wolf, Tandem use of optical sensing and machine learning for the determination of absolute configuration, enantiomeric and diastereomeric ratios, and concentration of chiral samples, *Angew. Chem., Int. Ed.*, 2020, **59**, 2440–2448.
7 W. Xu, M. Cheng, S. Zhang, Q. Wu, Z. Liu, M. K. Dhinakaran, F. Liang, E. G. Kovaleva and H. Li, Recent advances in chiral discrimination on host–guest functionalized interfaces, *Chem. Commun.*, 2021, **57**, 7480–7492.
8 Z. Li, Z. Mo, S. Meng, H. Gao, X. Niu and R. Guo, The construction and application of chiral electrochemical sensors, *Anal. Methods*, 2016, **8**, 8134–8140.
9 C. Pu, Y. Xu, Q. Liu, A. Zhu and G. Shi, Enantiomers of single chirality nanotube as chiral recognition interface for enhanced electrochemical chiral analysis, *Anal. Chem.*, 2019, **91**, 3015–3020.
10 R. M. Zawawi and A. L. T. Zheng, Zinc oxide/vancomycin-based electrochemical chiral sensor for the recognition of penicillamine enantiomers, *Int. J. Electrochem. Sci.*, 2020, **15**, 3255–3267.
11 S. Carradori, D. Secci, C. Faggi and R. Cirilli, A chromatographic study on the exceptional chiral recognition of 2-(benzylsulfinyl) benzamide by an immobilized-type chiral stationary phasebased on cellulose tris (3, 5-dichlorophenylcarbamate), *J. Chromatogr. A*, 2018, **1531**, 151–156.
12 X. Yu and Z. Yao, Chiral recognition and determination of enantiomeric excess by mass spectrometry: A review, *Anal. Chim. Acta*, 2017, **968**, 1–20.
13 J. Wei, Y. Guo, J. Li, M. Yuan, T. Long and Z. Liu, Optically active ultrafine Au-Ag alloy nanoparticles used for colorimetric chiral recognition and circular dichroism sensing of enantiomers, *Anal. Chem.*, 2017, **89**(18), 9781–9787.
14 C. Wang, E. Wu, X. Wu, X. Xu, G. Zhang and L. Pu, Enantioselective fluorescent recognition in the fluorous phase:enhanced reactivity and expanded chiral recognition, *J. Am. Chem. Soc.*, 2015, **137**(11), 3747–3750.
15 R. Wang, D. Sun, C. Wang, L. Liu, F. Li and Z. Tan, Biphasic recognition chiral extraction of threonine enantiomers in a two-phase system formed by hydrophobic and hydrophilic deep-eutectic solvents, *Sep. Purif. Technol.*, 2019, **215**, 102–107.
16 H. Xu, Y. Du, Z. Feng, Y. Du, Z. Feng, X. Sun and J. Liu, Synthesis of a chiral ionic liquid, cholinium-clindamycin phosphate,as sole chiral selector in capillary electrophoresis, *J. Chromatogr. A*, 2019, 460721.
17 E. Monteagudo, A. Virgili, T. Parella and M. Pérez-Trujillo, Chiral recognition by dissolution DNP NMR spectroscopy of 13C-labeled D/L-methionine, *Anal. Chem.*, 2017, **89**(9), 4939–4944.
18 O. A. Sadik, A. O. Aluoch and A. Zhou, Status of biomolecular recognition using electrochemical techniques, *Biosens. Bioelectron.*, 2009, **24**(9), 2749–2765.
19 T. Aree, R. Arunchai, N. Koonrugsa and A. Intasiri, Fluorometric and theoretical studies on inclusion complexes of β-cyclodextrin and d-, l-phenylalanine, *Spectrochim. Acta, Part A*, 2012, **96**, 736–743.
20 T. Polen, M. Krmer, J. Bongaerts, M. Wubbolts and V. F. Wendisch, The global gene expression response of Escherichia coli to L-phenylalanine, *J. Biotechnol.*, 2005, **115**, 221–237.
21 P. D. Kilcast, Psychophysical characterization of new sweeteners of commercial importance for the EC food industry, *Food Chem.*, 1996, **56**, 291–302.
22 L. X. Song, L. Zhao and Z. J. Guo, Inclusion Phenomena and Molecular Recognition of Cyclodextrin-Phenylalanine Supramolecular System, *Chin. J. Inorg. Chem.*, 2002, **09**, 897–901.
23 S. J. Liu, Q. Wen, L. J. Tang and J. H. Jiang, Phospholipid-graphene nanoassembly as a fluorescence biosensor for sensitive detection of phospholipase Dactivity, *Anal. Chem.*, 2012, **84**, 5944–5950.
24 H. Chen, M. B. Müller, K. J. Gilmore, G. G. Wallace and D. Li, Mechanically strong,electrically conductive and biocompatible graphene paper, *Adv. Mater.*, 2008, **20**, 3557–3561.
25 D. R. Dreyer, S. Park, C. W. Bielawski and R. S. Ruoff, The chemistry of graphene oxide, *Chem. Soc. Rev.*, 2010, **39**(1), 228–240.
26 A. Lerf, H. He, M. Forster and J. Klinowski, Strcture of graphite oxide revisited, *J. Phys. Chem. B*, 1998, **102**(23), 4477–4482.
27 S. Chen, J. Zhu, X. Wu and Q. Han, X. WangGraphene oxide—MnO2 nanocomposites for supercapacitors, *ACS Nano*, 2010, **4**(5), 2822–2830.
28 K. Nakada and M. Fujita, Edge state in graphene ribbons:Nanometer size effect and edge shape dependence, *Phys. Rev. B: Condens. Matter Mater. Phys.*, 1996, **54**(24), 17954–17961.
29 H. Gou, J. He, Z. Mo, X. Wei, R. Hu and Y. Wang, An electrochemical chiral sensor fortryptophan enantiomers based on reduced graphene oxide/1,10-phenanthroline copper(II)functional composites, *RSC Adv.*, 2015, **5**(74), 60638–60645.

30 C. Chen, W. Zhai, D. Lu, H. Zhang and W. Zheng, A facile method to prepare stable noncovalent functionalized graphene solution by using thionine, *Mater. Res. Bull.*, 2011, **46**(4), 583–587.
31 Y. L. Cui, B. Zhang, B. Q. Liu, H. F. Chen, G. N. Chen and D. P. Tang, Sensitive detection of hydrogen peroxide in foodstuff using an organic—inorganic hybrid multilayer-functionalized graphene biosensing platform, *Microchim. Acta*, 2011, **174**, 137–144.
32 K. S. Novoselov, A. K. Geim, S. V. Morozov, D. Jiang, Y. Zhang, S. V. Dubonos, *et al.*, Electric field effect in atomically thin carbon films, *Science*, 2004, **306**(5696), 666–669.
33 Q. Liu, A. Fei, J. Huan, H. Mao and K. Wang, Effective amperometric biosensor for carbaryl detection based on covalent immobilization acetylcholinesterase on multiwall carbon nanotubes/graphene oxide nanoribbons nanostructure, *J. Electroanal. Chem.*, 2015, **740**, 8–13.
34 J. S. M. A. Akter, Ultrasensitive Nanoimmunosensor by coupling non-covalent functionalized graphene oxide platform and numerous ferritin labels on carbon nanotubes, *Biosens. Bioelectron.*, 2016, **80**, 123–130.
35 Y. J. Wan, W. H. Yang, S. H. Yu, R. Sun, C. P. Wong and W. H. Liao, Covalent polymer functionalization of graphene for improved dielectric properties and thermal stability of epoxy composites, *Compos. Sci. Technol.*, 2016, **122**, 27–35.
36 L. Cao, Q. Sun, Y. Gao, L. Liu and H. Shi, Novel acid-base hybrid membrane based on amine-functionalized reduced graphene oxide and sulfonated polyimide for vanadium redox flow battery, *Electrochim. Acta*, 2015, **158**, 24–34.
37 R. S, B. X. Li and L. Zhang, Visual detection of hexokinase activity and inhibition with positively charged gold nanopartic1es as colorimetric probes, *Analyst*, 2013, **138**, 3142–3145.
38 Y. S. Xia, Y. L. Zhou and Z. Y. Tang, Chiral inorganic nanoparticles: Origin, optical properties and bioapplications, *Nanoscale*, 2011, **3**, 1374–1382.
39 P. Hohenberg and W. Kohn, Inhomogeneous Electron Gas, *Phys. Rev.*, 1964, **136**, B864–B871.
40 W. Kohn and L. J. Sham, Self-Consistent Equations Including Exchange and Correlation Effects, *Phys. Rev.*, 1965, **140**, A1133–A1138.
41 G. Kresse and J. Furthmüller, Efficient iterative schemes for *ab initio* total-energy calculations using a plane-wave basis set, *Phys. Rev. B: Condens. Matter Mater. Phys.*, 1996, **54**, 11169.
42 P. E. Blöchl, Projector augmented-wave method, *Phys. Rev. B: Condens. Matter Mater. Phys.*, 1994, **50**, 17953–17979.
43 A. I. Kozlov, A. P. Kozlova, H. C. Liu and Y. Iwasawa, A new approach to active supported Au catalysts, *Appl. Catal., A*, 1999, **182**(1), 9–28.
44 C. Burda, T. Green, C. Landes, S. Link, R. Little, J. Petroski and M. A. El-Sayed, *Optical Spectroscopy of Nanophase Material*, Wiley-VCH Verlag GmbH, 2001.
45 H. C. Hulst Vande, *Light Scattering by Small Particles*, John Wiley & Sons Dover Publications, New York, 1957.
46 I. S. Lim, D. Mott, M. H. Engelhard, Y. Pan, S. Kamodia, J. Luo, P. N. Njoki, S. Q. Zhou, L. C. Wang and C. J. Zhong, Interparticle chiral recognition of enantiomers: a nanoparticle-based regulation strategy, *Anal. Chem.*, 2009, **81**(2), 689–698.
47 W. S. Hummers and R. E. Offeman, Preparation of graphitic oxide, *J. Am. Chem. Soc.*, 1958, **80**, 1339.
48 K. C. Grabar, R. G. Freeman, M. B. Hommer and M. J. Natan, Preparation and characterization of Au colloid monolayers, *Anal. Chem.*, 1995, **67**, 735–743.